Appendix 5

Appendix 3

A generalized jet-sink model for tidal exchange in coastal inlets

Background

The goal of this work is to formulate a simple model of the tidal exchange between a bay and the ocean which accounts for effects of ambient cross-flow, tidal range, and stratification. The model is based on the idea first proposed by Stommel and Farmer (1952), that the exchange is regulated by the asymmetry between the ebb and flood tides. Their simple model assumed a rectangular jet for the outflow from the bay, and a potential sink for the inflow. The water returning to the bay on the inflow was assumed to be drawn from the region of this sink which overlaps with the plan-form of the ebb jet (Figure 1). They went on to show how the steady-state salt balance of an estuary could be controlled by this mechanism by limiting the amount of saline ocean water available on each tidal exchange. Ozsoy (1977) extended this work by assuming the outflow satisfied an analytical solution for shallow water, turbulent jets and presented results which showed the effect of varying tidal range and bottom friction. Wilkenson (1978) performed laboratory studies of periodic exchange for an unstratified inlet and found that the net exchange was strongly influenced by the tidal range. Numerical studies by Signell and Butman (1992) showed that this type of mechanism also controlled the exchange at the mouth of Boston Harbor, though the prototype topography was significantly more complex and no ambient ocean currents were imposed. Observational studies of inlets have focused primarily on the outflow structure (e.g. Taylor and Dean, 1974, Unluata and Ozsoy, 1977, Hearn et al., 19xx, ...), with few direct measures of net tidal exchange.

This work builds on the previous work of Stommel and Farmer (1952), and Ozsoy (1977) to incorporate the effects of cross flow, tidal range, topography and stratification into a generalized, jet-sink model. To do this, the analytical solutions for a jet with cross flow and varying bottom topography are coupled with a potential flow solution to from a quasi-steady jet-sink model for the tidal exchange problem. The exchange fraction, or tidal exchange ratio (TER), is found by determining the portion of the mass ejected by the ebb jet that is returned within the withdrawal zone of the subsequent flood tide (Fischer et al., 1979). The purpose of this model is to allow simple comparisons of the relative effects of a range of controlling parameters on the TER for inlets with simple topography.

Model Formulation - Ebb Jet

Following Ozsoy (1977), the outflow jet with cross-flow, bottom friction, variable bottom topography, and lateral entertainment can be described by a set of 5 simultaneous, ordinary, differential equations based on the depth integrated shallow water equations as follows,

$$\frac{d}{d\xi_*}(\overline{I_1}HBU) = \alpha HU \tag{1}$$

$$\frac{d}{d\xi_*}(\overline{I_2}HBU^2) = \alpha\, HU_A U\cos\theta - \mu\overline{I_2}BU^2 \tag{2}$$

$$\overline{I_2}BU\frac{d\theta}{d\xi_*} = -\alpha\, U_A \sin\theta \tag{3}$$

$$\frac{d\xi}{d\xi_*} = \sin\theta \tag{4}$$

$$\frac{d\chi}{d\xi_*} = \cos\theta \tag{5}$$

where $H=h/h_o$ is the depth, $B=b/b_o$ is the jet half width, $U=u/u_o$ is the centerline velocity, α is the entertainment coefficient, θ is the jet deflection angle, $\xi=x/b_o$ is the offshore coordinate, $\chi=y/b_o$ is the longshore coordinate, and $\xi_*=x_*/b_o$ is the corresponding curvilinear offshore coordinate that follows the jet bending. All variable are non-dimensionalized by the conditions at the jet origin, u_o, b_o, h_o. Equation (1) arises from continuity, while (2) and (3) are the streamwise and lateral momentum equations, and (4) and (5) relate the cartesian and curvilinear coordinate systems. $\overline{I}_1$ and $\overline{I}_2$ are defined by the integral formulas

$$\overline{I_1} = \int_0^1 (\frac{u}{u_c}) d\zeta \tag{6}$$

$$\overline{I_2} = \int_0^1 (\frac{u}{u_c})^2 d\zeta \tag{7}$$

and the velocity profile is assumed to be self-similar such that

$$\frac{u}{u_c} = \frac{U_A}{U}\cos\theta\,[1 - F(\zeta)] + F(\zeta) \tag{8}$$

where $\zeta=y_*/b$ is the local lateral coordinate for the bending jet and $F(\zeta)$ is a similarity function based on experimental data (e.g. Stolzenbach and Harleman, 1971, Abramovich, 1963) and taken to satisfy

$$F(\zeta) = \begin{cases} 0 & ;|\zeta| > B \\ (1-\zeta_o^{1.5})^2 & ; R<|\zeta|<B,\ \ \zeta_o = \dfrac{|\zeta|-R}{B-R} \\ 1 & ;\ 0<|\zeta|<R \end{cases} \tag{9}$$

in the zone of flow establishment (ZOFE) and

$$F(\zeta) = \begin{cases} 0 & ;|\zeta| > B \\ (1-\zeta^{1.5})^2 & ; 0<|\zeta|<B \end{cases} \tag{10}$$

in the zone of established flow (ZOEF).

The solution is subject to several assumptions including that steady state conditions hold, water depth is small compared to the horizontal length scale but large compared to the length scale of vertical motions, no surface shear or atmospheric pressure gradients, turbulent diffusivities much larger than molecular, surface displacements are small compared to depth, a quadratic bottom friction law, self-similarity, jet bending is gradual, entertainment velocity proportional to centerline velocity, entertainment doesn't modify the cross flow significantly, and potential flow outside the jet region. Examples of the flow structure resulting from this solution are shown in Figure 2.

The concentration distribution in the jet is also taken to be self-similar but the similarity function is slightly different than (9)-(10) with

$$\frac{c}{c_c} = \frac{C_A}{C}[1-G(\zeta)]+G(\zeta) \tag{11}$$

and

$$G(\zeta) = \sqrt{F(\zeta)} \tag{12}$$

Typical concentration distributions within the outflowing jet are superimposed on the velocity field in Figure 2. The original jet equations are solved by reformulation into a finite difference scheme where

$$(\overline{I_1}HBU)_i = (\overline{I_1}HBU)_{i-1} + (\alpha HU)_{i-1}\Delta\xi. \tag{13}$$

$$(\overline{I_2} HBU^2)_i = (\overline{I_2} HBU^2)_{i-1} + (\alpha HU_A U\cos\theta - \mu \overline{I_2} BU^2)_{i-1}\Delta\xi_* \quad (14)$$

$$\theta_i = \theta_{i-1} + (\frac{-\alpha U_A \sin\theta}{\overline{I_2} BU})_{i-1}\Delta\xi_* \quad (15)$$

The boundary conditions for the ZOFE require H=B=1 and θ=0 at ξ_*=0 and U=1 throughout. For the ZOEF, the boundary conditions are specified by the values of H and B at the end of the ZOFE where R=0 and U=1. The bottom slope is taken to be linear so that H can be written as

$$H = 1 + H_x\xi \quad (16)$$

where H_x is the non-dimensional bottom slope $(dh/dx)(b_o/h_o)$.

The Flood Sink

For slowly varying topography, the flood flow can be described by a potential function (e.g. Wolanski, 1984, Oszoy, 1977) of the form

$$hu = \frac{\delta\phi}{\delta x}, \quad hv = \frac{\delta\phi}{\delta y} \quad (17)$$

which satisfies the irrotationality condition

$$\frac{\delta v}{\delta x} - \frac{\delta u}{\delta y} = 0 \quad (18)$$

so long as the bottom slopes satisfy $(h_x,h_y)<<(h_o/b_o)$. The potential flow solution for the flood flow can be formulated in polar coordinates (r,θ) as a superposition of a potential sink,

$$\phi_S = \Gamma_o \ln(r) \quad (19)$$

and a uniform ambient cross flow,

$$\phi_A = U_A r\cos\theta \tag{20}$$

to yield a combined description of the flow which must satisfy,

$$\phi = \Gamma_o \ln(r) + U_A r\cos\theta \tag{21}$$

Where Γ_o is the strength of the sink and is related to the boundary conditions by $\Gamma_o = u_o h_o b_o/\pi$.

From the definition of the potential function, the velocity field can be found as

$$u_r = u_A\cos\theta - \frac{\Gamma_o}{rh} \tag{22}$$

$$u_\theta = -u_A\sin\theta \tag{23}$$

Non-dimensionalizing and changing to cartesian coordinates

$$U = \frac{\Gamma_o \xi}{\xi^2 + \chi^2} \tag{24}$$

$$V = V_A + \frac{\Gamma_o \chi}{\xi^2 + \chi^2} \tag{25}$$

The flood withdrawal zone is then determined numerically by finding the initial positions of a set of particles which are advected to the mouth during the tidal period T according to,

$$\chi_i = \chi_{i-1} - U_o\left[U_a + \frac{1}{\pi}\left(\frac{\chi_{i-1}}{(1 + H_x\chi_{i-1})(\chi^2_{i-1} + \xi^2_{i-1})}\right)\right]\Delta\tau \tag{26}$$

$$\xi_i = \xi_{i-1} - \frac{1}{\pi}\left(\frac{\xi_{i-1}}{(1 + H_x\chi_{i-1})(\chi^2_{i-1} + \xi^2_{i-1})}\right)\Delta\tau \tag{27}$$

The plan form view of the resulting flood-tide withdrawal zone for a typical inflow condition is shown in Figure 3.

Buoyancy Effects

If the ebb jet is buoyant relative to the ambient water, the flow may lift off the bottom at some point outside the entrance. This effect has been demonstrated in both laboratory (Armi, 1986, Safie, 1979) and prototype systems (Hearn et al, 198?, Chadwick et al., 1994). Several criteria have been suggested to predict the point at which lift off will occur including those based on jet exit conditions (Safie, 1979, Hausenstien, 19??) and those based on local flow conditions (Hearn et al., 198?). For our simple model we adopt the criteria of Hausenstien

$$H_{liftoff} = 0.71\, Fr_o\, H_x^{1/4} \tag{28}$$

where $H_{liftoff}$ is the liftoff depth, $Fr_o = u_o/(g'h_o)^{1/2}$ is the exit Froude number, g' is the reduced gravity, and H_x is the bottom slope as before. Thus for a given topography, the liftoff depth can be predicted from the exit Froude number of the ebb flow. To incorporate this into the exchange model, we assume that, following liftoff, the bottom interface of the ebb jet continues off shore at a constant depth equal to $H_{liftoff}$. The case of liftoff inside the entrance is not considered. The jet is then characterized using this new depth profile. On the return flow, both the water within the upper layer from the ebb flow, and the static water in the lower layer beneath are assumed to be drawn back into the inlet, along with the remaining water in the lateral regions of the withdrawal zone (Figure 4). This produces two competing effects with respect to exchange. First, the additional water drawn in from beneath the outflow jet should increase the exchange efficiency. Second, the widening of the jet caused by the shallower depth of the lifted interface should reduce the flushing efficiency.

Tidal Exchange Model

The jet-sink, tidal-exchange model is formulated by determining the amount of bay water ejected by the ebb jet into the flood withdrawal zone. This is done by calculating numerically the ratio of bay water in the withdrawal zone to total water in the withdrawal zone (Figure 5). The solution set is then explored by varying the set of four non-dimensional controlling parameters

$$TER = F(U_o, U_A, H_x, Fr_o) \tag{29}$$

Here $U_o=u_oT/b_o$ is essentially the aspect ratio of the ebb jet since $u_oT=L_o$ is the length scale of the periodic tidal jet. The parameter U_A is simply the ratio of the cross flow velocity to the tidal velocity as previously defined, H_x is the bottom slope in terms of depth increases per entrance width offshore, and Fr_o is the exit Froude number described above.

The model is simplistic in the sense that it neglects effects due to unsteady behavior of the flow, inertial effects especially in the jet, spatial and temporal variations in the cross flow, complexities in the topography, and vertical mixing. Previous studies of tidal jets have shown that one of the primary results of the periodic nature of the jet is the generation of vortex pairs which tend to entrain the fluid ejected by the jet (e.g. Wilkenson, 1978, Hearn et al., 19xx) . These vortices may migrate offshore due to their self induced velocity, be advected by the ambient flow, or be drawn back by the flood flow. Their lifetime is thought to be determined primarily by spindown due to bottom friction (Van Sender and Imberger, 1990).

Inertial effects in the jet will generally tend to enhance the offshore ejection of bay water in the central core of the jet, while reversal and inflow occurs first at the channel edges of the entrance. This can lead to increased exchange, because the water at the periphery will generally be of oceanic origin. The ambient flow may or may not be steady, and may exhibit significant spatial gradients both in the vertical and horizontal planes. Often, the coastal flow may contain a strong tidal component which may or may not be phase-locked with the tidal currents at the mouth. These variations, combined with increasing complexity of the shoreline and bottom topography can make the ambient flow difficult to interpret within such a simple model. The aim of this work is not to resolve these complexities, but only to provide a framework for evaluating relative effects of various forcing terms, and exploring the basic mechanisms by which they influence tidal exchange.

Results

Results for a range of solutions are presented in Figures 5-7. In each case, the cross flow parameter U_A was varied between -1 and 1 generating symmetrical solutions for cross flows ranging between zero, and equal to the tidal strength in both longshore directions. The solutions are symmetrical because the topography is taken to be a simple, straight coastline (e.g. Figure 1).

In the first series (Figure 5a), the tidal range parameter U_o (aspect ratio) was varied between about 5 and 50 where 5 would indicate weak or neap tidal forcing, and 50 would indicate strong or spring tide conditions. The bottom slope was held flat (H_x=0), and no liftoff condition was imposed (unstratified). The results show that the tidal exchange varies considerably over this range with maximum exchange on strong tides with strong cross flows. On the weak tides, the tidal exchange is reduced by as much as 60%. The reason for this is illustrated by Figure 5b which shows the variation in the exchange zone between weak and strong tides. From this sequence of plots it is clear that during weak tides, a much larger fraction of the withdrawal zone is occupied by bay water than during strong tides. There appears to be little coupling between tidal strength and cross flow, so that variations in cross flow produce the same effect on exchange independent of the tidal range. Figure 5a shows that increasing the cross flow U_A from 0 to 1 results in an increase in exchange efficiency from between 15-25% with slightly stronger effects during weaker tidal range. The effect of cross flow on the exchange is illustrated in Figure 5c which shows how the jet bends off and the withdrawal zone becomes narrower in the offshore direction as cross flow is increased resulting in a smaller exchange zone.

In the second series, the bottom slope parameter H_x was evaluated for values between 0 and 1 (Figure 6a). Recall that the potential flow solution is only strictly valid for $H_x << 1$. The tidal velocity was fixed at U_o=21.6, and again no liftoff was considered. The results show that increasing slope offshore results in significantly greater exchange. As shown in Figure 6b, this appears to result from a narrowing of the jet as it moves offshore over strongly sloping bottom, combined with a narrowing of the withdrawal zone offshore. There is a definite coupling between the cross flow and the bottom slope effects. As cross flow strengthens, the effects of

bottom slope are diminished. This may be due to the effective shortening of the withdrawal zone by the cross flow, thus reducing the effectiveness of the bottom slope. Variations in H_x can perhaps also be used as a first order indication of effects of liftoff due to stratification. This would presume that the bottom layer over which the ebb jet flows remains essentially static during the flood tide as well and hence the main effect of the liftoff is to change the planform of the outflow. This would suggest that buoyancy driven liftoff could lead to a reduction in exchange.

In the third series, the outflow Froude number was varied between 0.5 and 5.5. For this case, the bottom slope was set to H_x=1, and the tidal velocity was held constant at U_o=43.2. The results show that the effects of stratification are limited to a range of Froude numbers such that liftoff of the jet occurs at a distance ranging from the entrance, to the outer extent of the withdrawal zone. If liftoff occurs outside the withdrawal zone, then no effect on exchange takes place. Even in the range where stratification effects the exchange, the response is weak. This appears to be due to a competition between the vertical exchange due to liftoff and the lateral variations in jet width caused by the liftoff. The first effect leads to additional ocean water being drawn in from beneath the outflow jet thus increasing the exchange efficiency. On the other hand, the widening of the jet caused by the shallower depth of the lifted interface reduces the flushing efficiency. The effects of stratification appear to be enhanced by cross flow.

Conclusions

The basic conclusions from this simple modeling approach indicate that,

1. Variations in tidal exchange are strongly influenced by spring-neap cycles, with most efficient exchange during strong tides and reductions in exchange of as much as 60% during neap tide conditions.

2. Cross-flow driven by ambient currents also results in a significant increase in exchange efficiency with exchange increasing over the no cross flow condition by 15-25% when cross flow is of equal strength to tidal flow.

3. Topographic effects due to bottom slope also effect exchange with increasing bottom slope leading to enhanced exchange efficiency.

4. First order effects of outflow liftoff due to stratification appear to have a limited effect on exchange as the competing influence of increased vertical exchange and decreased lateral exchange tend to cancel out.

References

Armi, L. and D. Farmer, 1986. Maximal two-layer exchange through a contraction with barotropic net flow. *J. Fluid Mech.*, **164**:27-51.

Fischer, H.B., List, E.J., Koh, R.C.Y., Imberger, J., and Brooks, N.H. 1979. Mixing in inland and coastal waters. Academic Press, San Diego, 483 pp.

Joshi, P.B. 1982. Hydromechanics of tidal inlets. *Journal of Port, Waterway, Harbor, and Ocean Division*, ASCE, **108**(WW3):239-253.

Largier, J.L., C.J. Hearn, and D.B. Chadwick, 1995a. Density structures in low-inflow, seasonal estuaries. Submitted to: Proceedings of the 7th International Biennial Conference on Physics of Estuaries and Coastal Seas, November, 1994, Woods Hole, MA.

Largier, J.L., J.T. Hollibaugh, and S.V. SMith, 1995b. Seasonally hypersaline estuaries in mediterannean climatic regions. Submitted to: Estuarine, Coastal and Shelf Science.

Ozsoy, E. 1977. Flow and mass transport in the vicinity of tidal inlets. University of Florida, Gainesville, Coastal and Oceanographic Engineering Department, Report #UFL/COEL/TR-036.

Safaie, B. 1979. Mixing of buoyant surface jet over sloping bottom. *Journal of Port, Waterway, Harbor, and Ocean Division*, ASCE, **105**(WW4):357-373.

Signell, R.P. and B. Butman,1992. Modeling tidal exchange and dispersion in Boston Harbor. J. Geophys. Res., 97(C10):15591-15606.

Stommel, H. and Farmer, H.G. 1952. On the nature of estuarine circulation. Woods Hole Oceanographic Inst. References Nos. 52-51, 52-63, 52-88.

Taylor, R.B. and Dean, G. 1974. Exchange characteristics of tidal inlets. *Proc. Coastal Eng. Conf.*, ASCE, **14**:2268-2289.

Unluata, U.A. and Ozsoy, E. 1977. Tidal jet flows near inlets. *Hydraulics in the Coastal Zone*, ASCE, pp 90-98.

Van Sender, D.C. and Imberger, J. 1990. Effects of initial conditions and Ekman suction on tidal outflows from inlets. *J. Geophys. Res.*, **95**(C8):13373-13391.

Wilkenson, D.L. 1978. Periodic flows from tidal inlets. *Proc. Coastal Eng. Conf.*, ASCE, **16**(2):1336-1346.

Wolanski, E.J. and Imberger, J. 1987. Friction-controlled selective withdrawal near inlets. *Estuarine, Coastal and Shelf Science*, **24**:327-333.

List of Figures

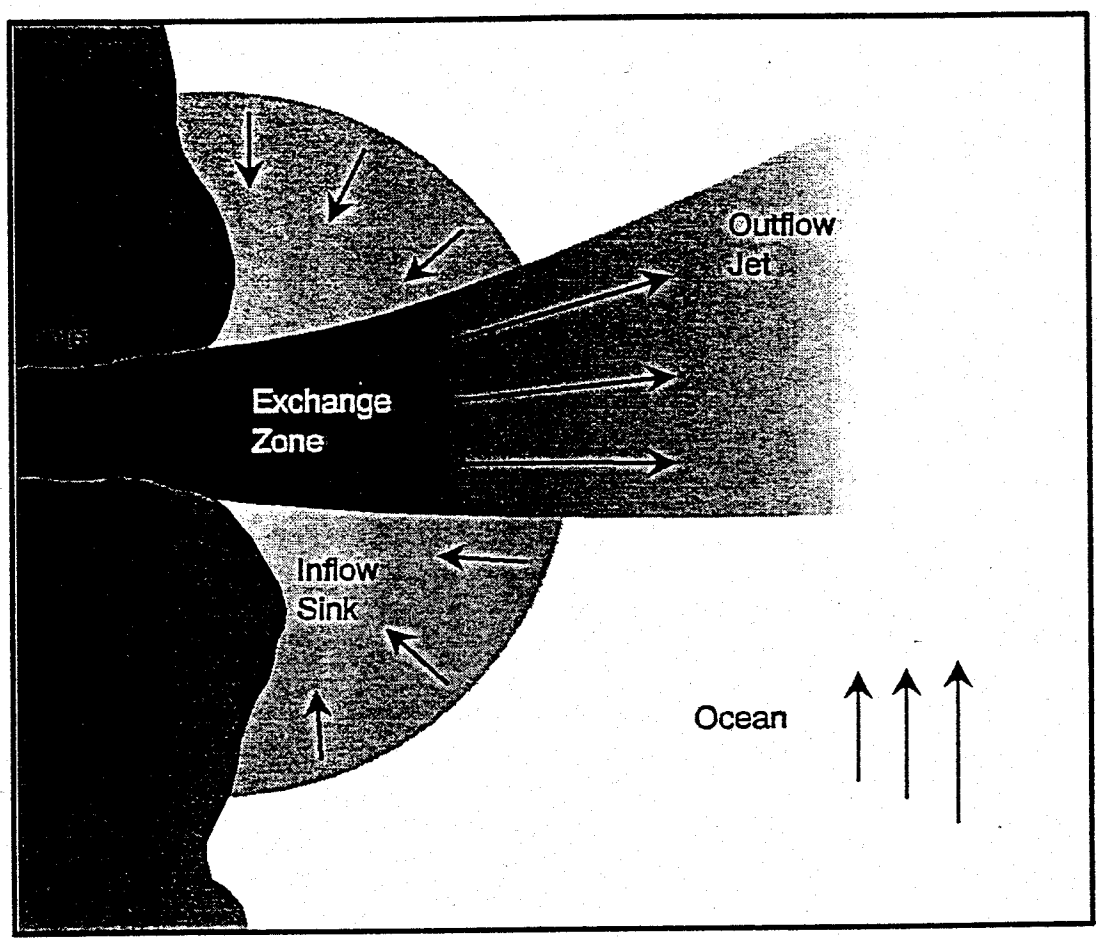

Figure 1.

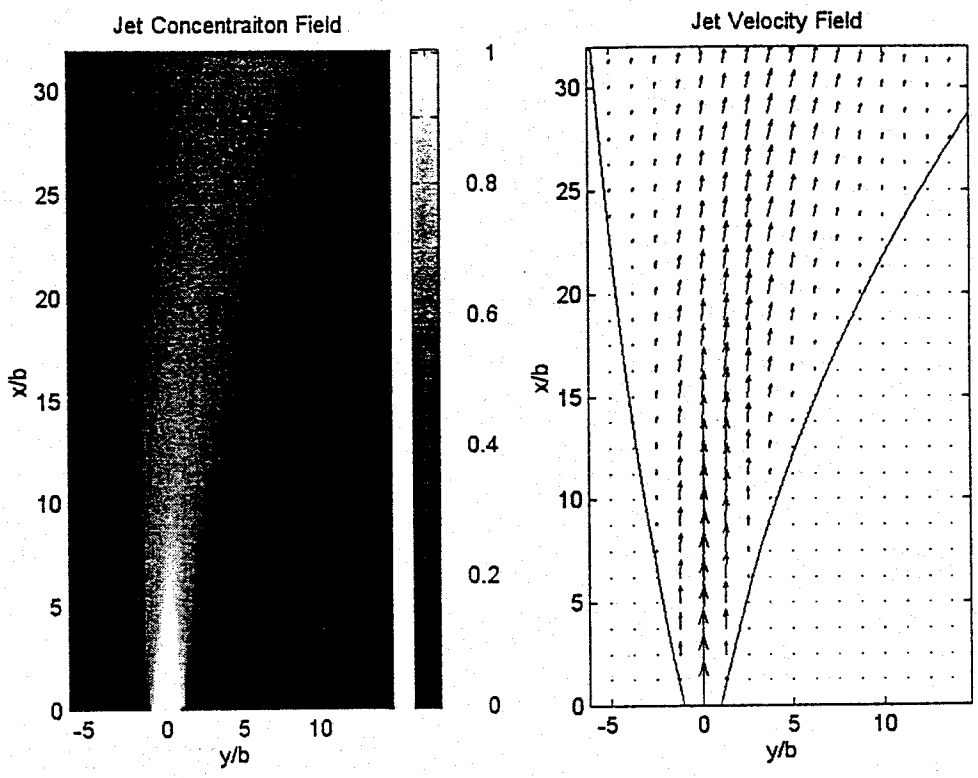

Figure 2.

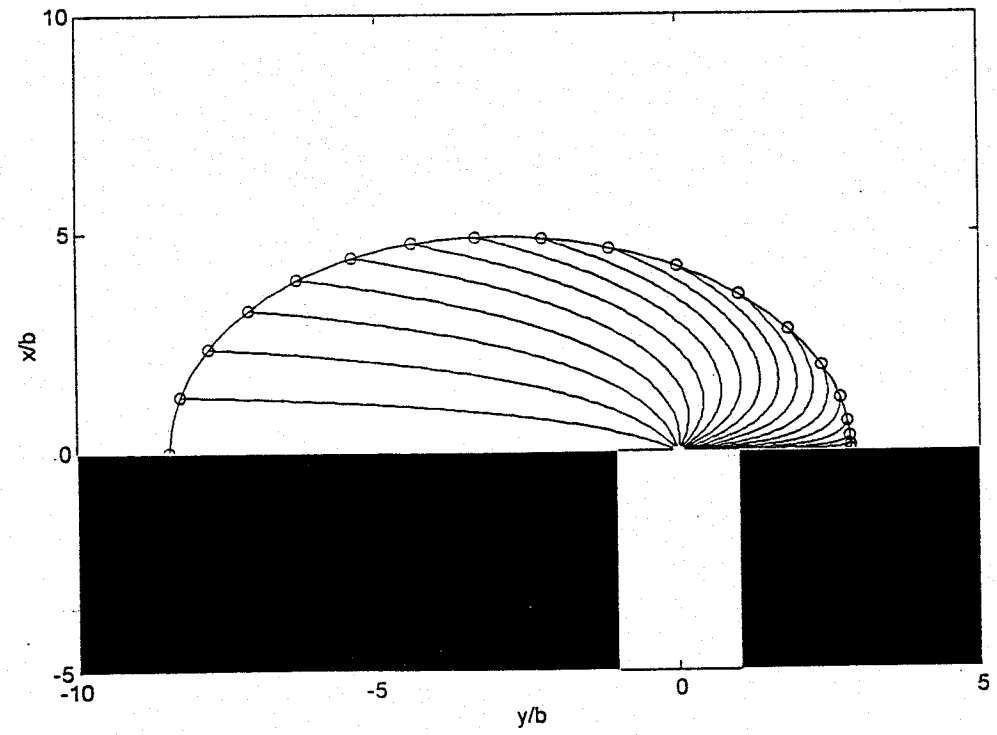

Figure 3.

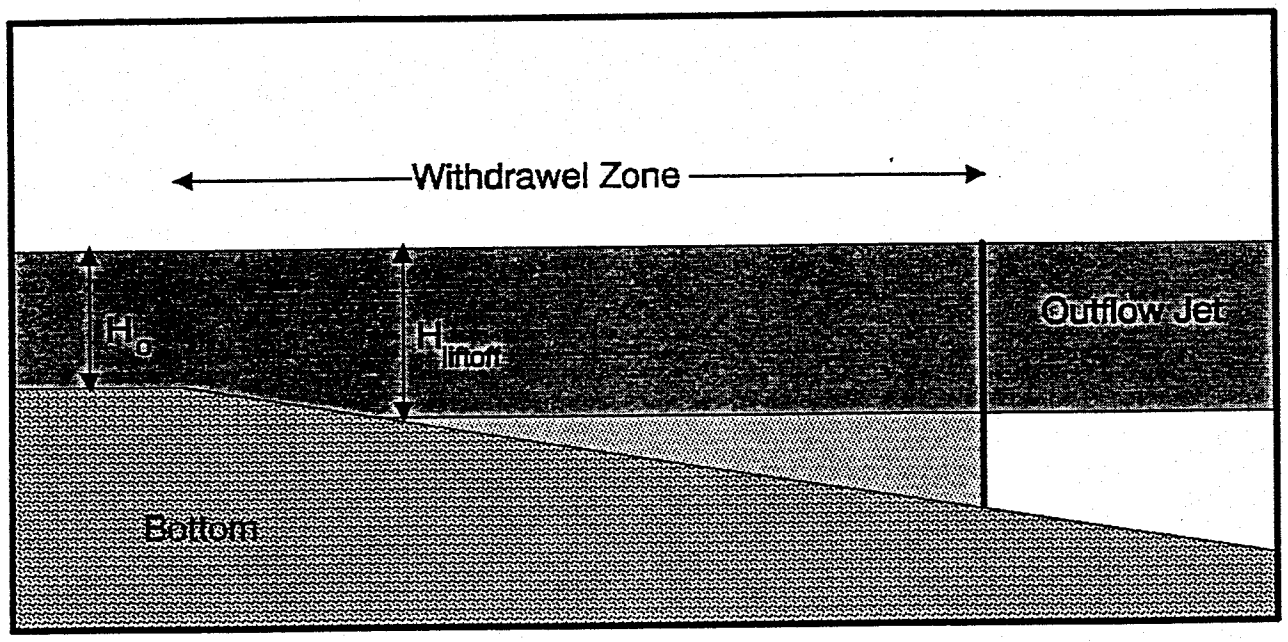

Figure 4.

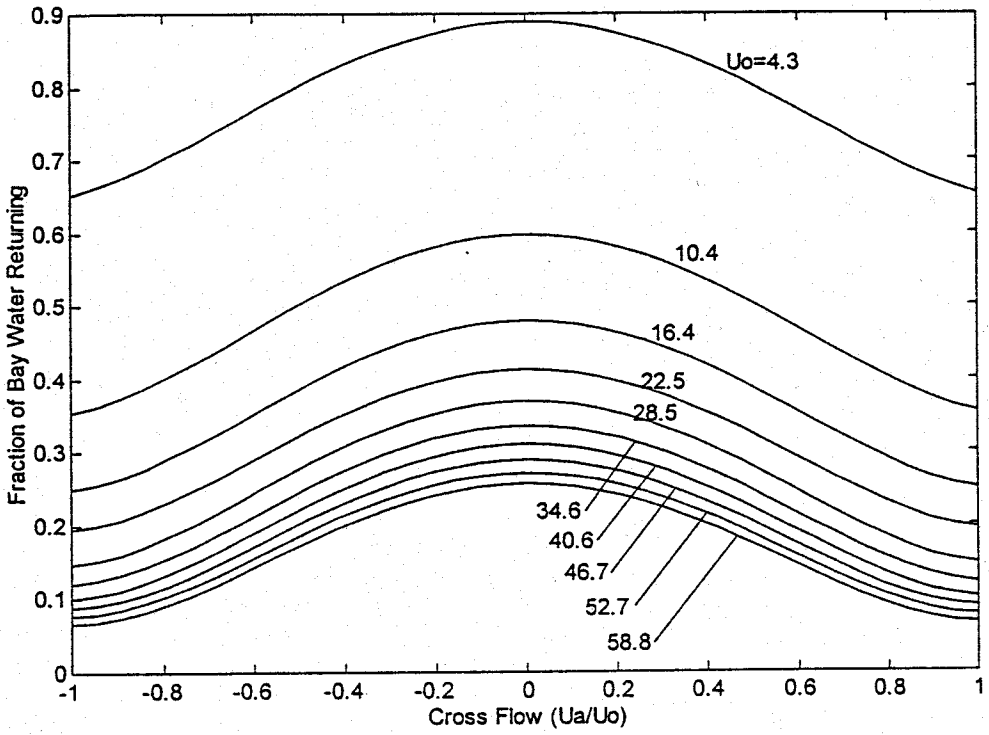
Fraction of Bay Water Returning
Cross Flow (Ua/Uo)
Uo=4.3
10.4
16.4
22.5
28.5
34.6
40.6
46.7
52.7
58.8
0
0.1
0.2
0.3
0.4
0.5
0.6
0.7
0.8
0.9
-1
-0.8
-0.6
-0.4
-0.2
0
0.2
0.4
0.6
0.8
1

Figure 5a.

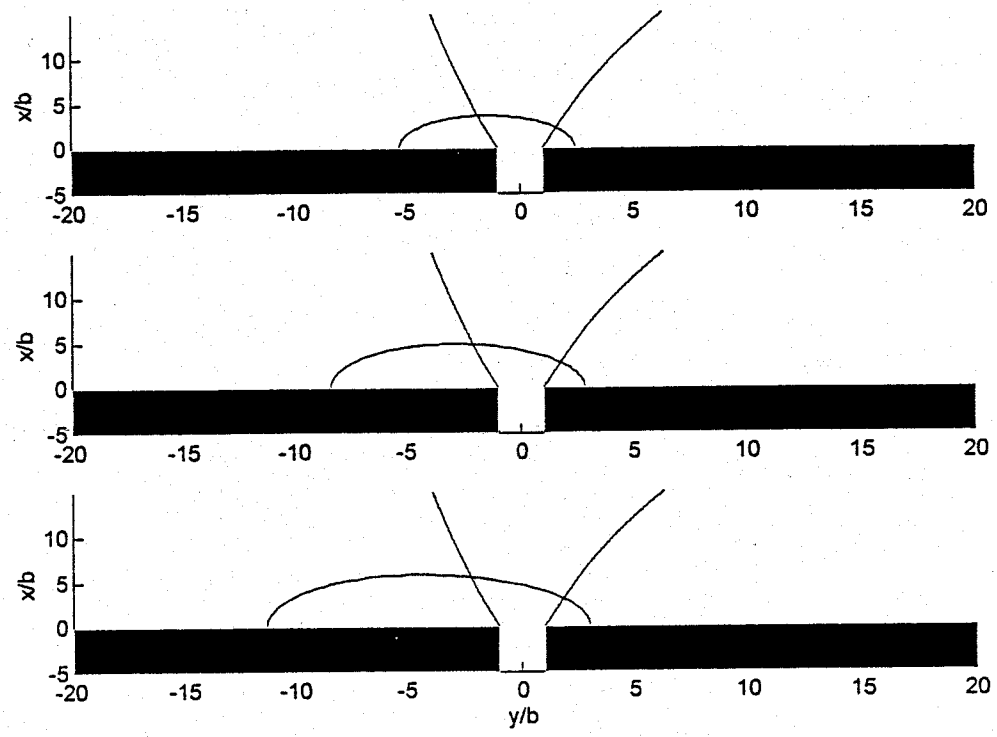

Figure 5b.

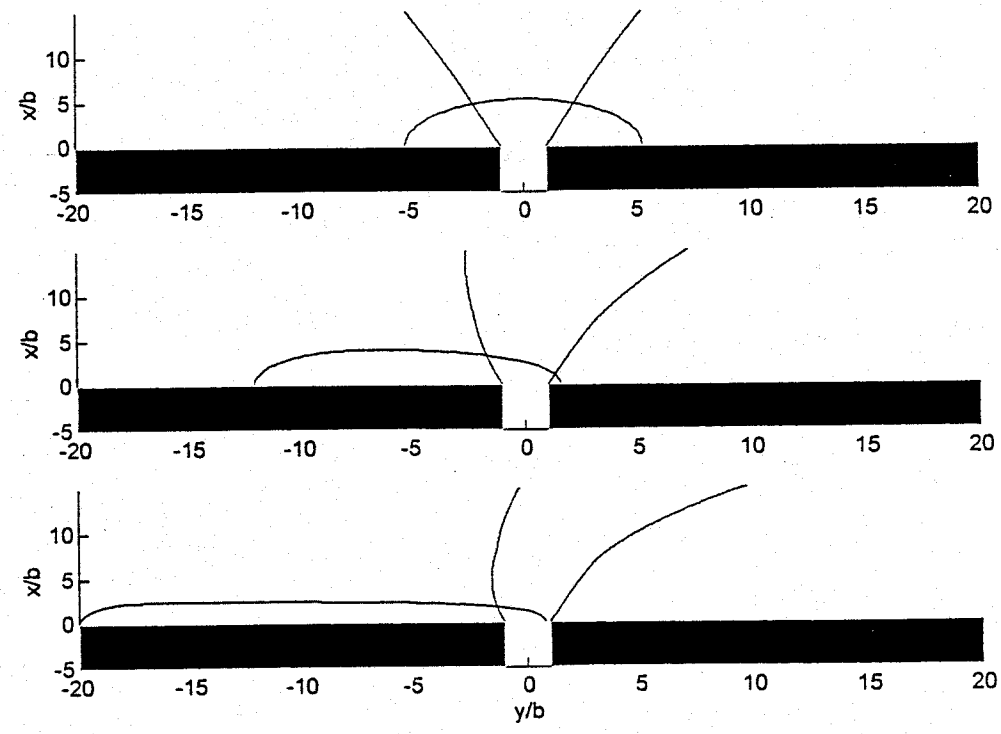

Figure 5c.

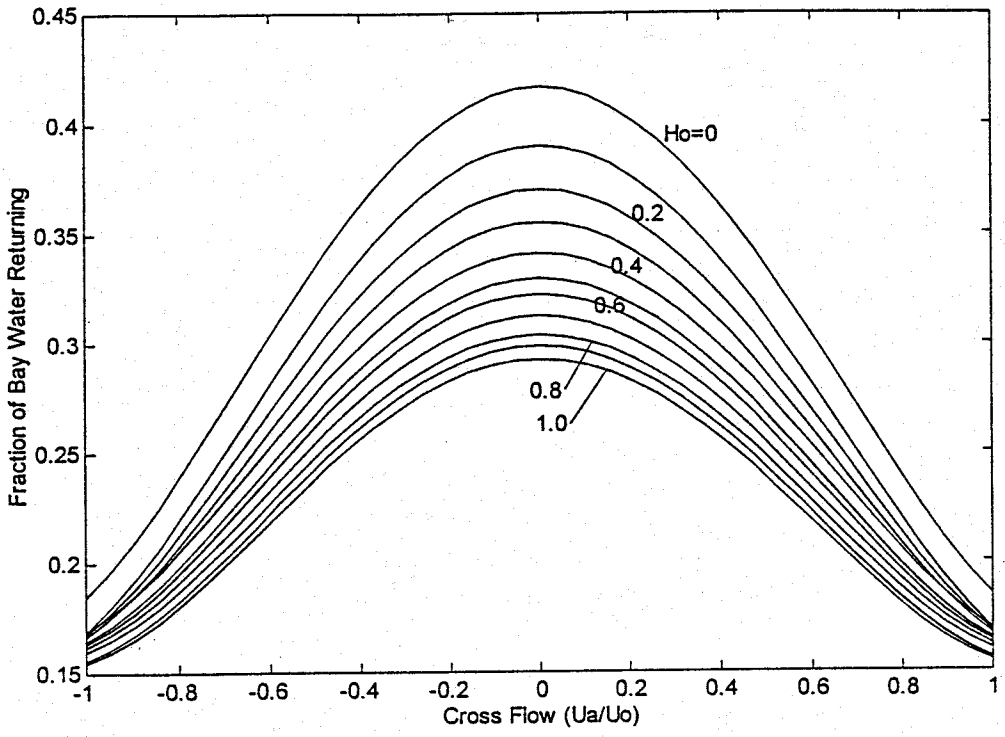

Figure 6a.

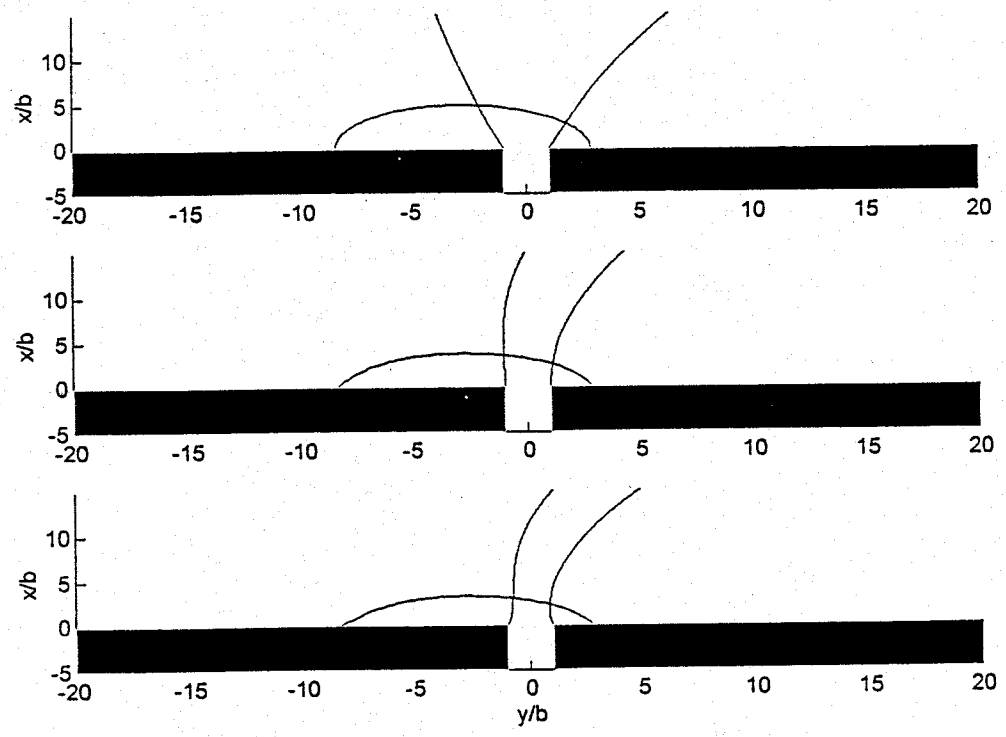

Figure 6b.

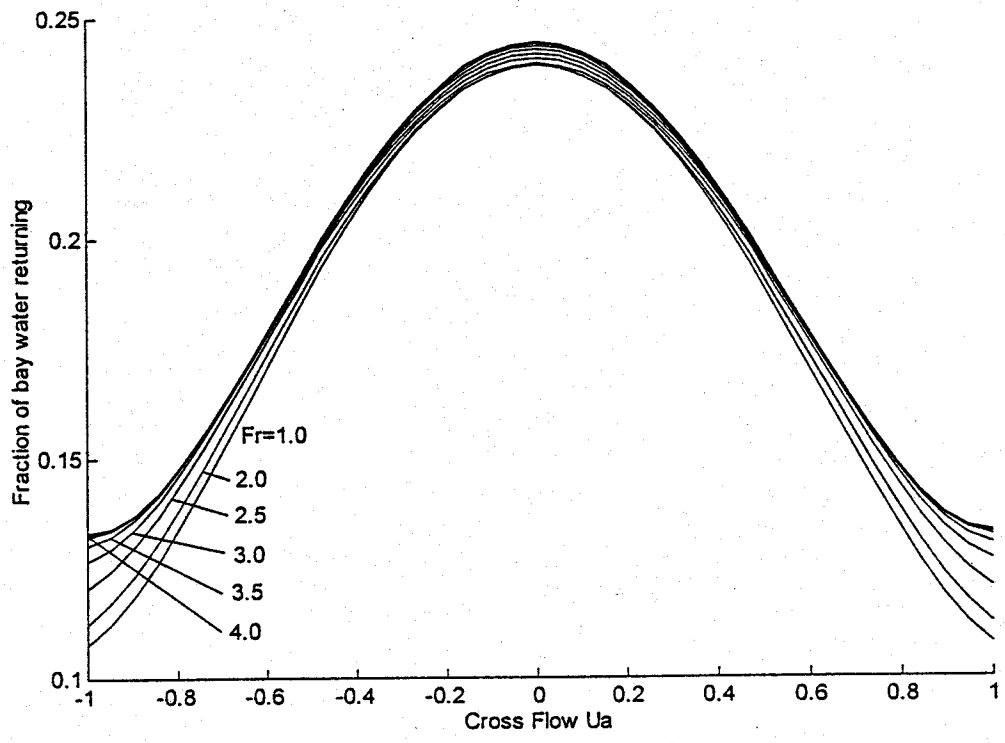

Figure 7a.

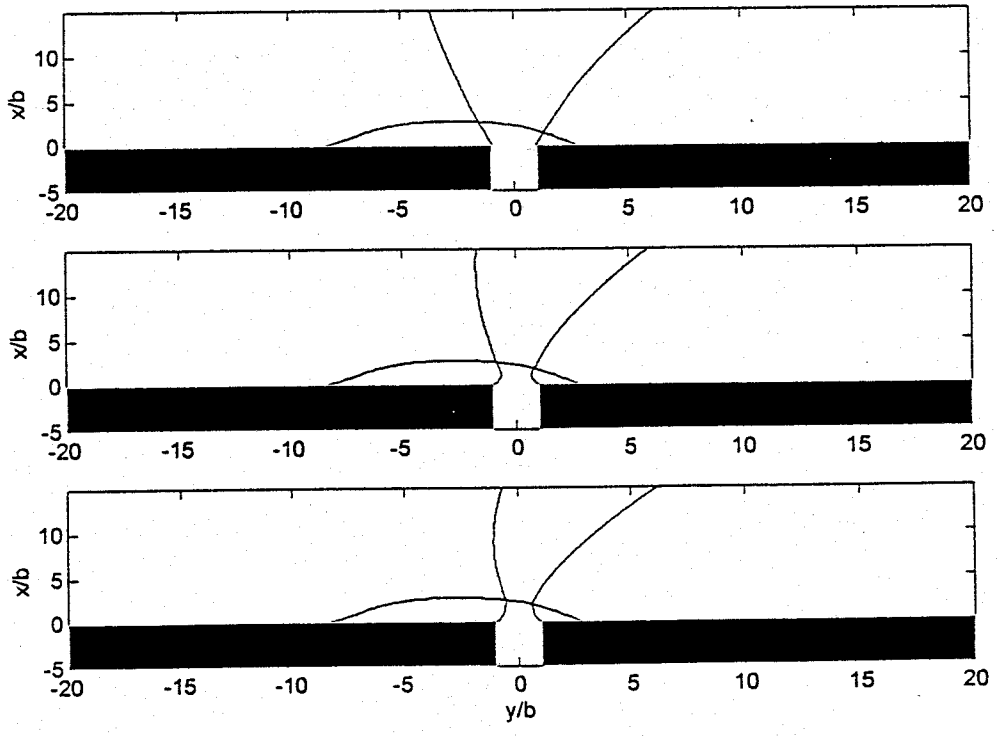

Figure 7b.

Appendix 6

Appendix G

CONTAMINANT TRANSPORT MEASUREMENTS IN SAN DIEGO BAY

Bart Chadwick[1], Charles Katz[2] and John Largier[3]

[1]Environmental Sciences Division, NCCOSC RDT&E Division, San Diego, CA
[2]Computer Science Corporation, San Diego, CA
[3]Center for Coastal Studies, Scripps Institute of Oceanography, San Diego, CA

ABSTRACT

In this paper, a method is described by which the tidal transport of petroleum hydrocarbons is measured directly at several sections within San Diego Bay. The resulting data set is unique in that it provides a quantitative means for estimating contaminant transport and tidal flushing. The measurements were obtained with a combination of shipboard instrumentation including an acoustic Doppler current profiler (ADCP), a profiling conductivity, temperature, and depth system (CTD), and a flow-through ultraviolet fluorometer (UVF) installed aboard the Navy's environmental survey craft RV ECOS. Cross sectional transects at five stations in San Diego Bay were performed to determine the net tidal transport of petroleum hydrocarbons. From the results, estimates of contaminant fluxes through the bay were made. The transport fluxes were compared to estimated inputs to the bay. Tidal exchange between the bay and ocean was evaluated and residence times for various portions of the bay were estimated.

INTRODUCTION

Pollution transport in bays and estuaries is often difficult to characterize due to the complexity of the processes which control the transport. Most studies of contaminant transport resort to numerical simulations of the flow and dispersion processes which determine the ultimate fate of the material (e.g. Signell and Butman, 1992; Sutton et al., 1995). While numerical models often provide useful and interesting results, they are generally difficult to validate. This is due to the problems associated with measuring flow and contamination levels over appropriate temporal and spatial scales. In this paper, a method is described by which the tidal transport of petroleum hydrocarbons is measured directly at several sections within San Diego Bay. The measurements were obtained with a combination of shipboard instrumentation including an acoustic Doppler current profiler (ADCP), a profiling conductivity, temperature, and depth system (CTD), and a flow-through ultraviolet fluorometer (UVF) installed aboard the Navy's environmental survey craft RV ECOS (Chadwick and Salazar., 1991). Cross sectional transects at five stations in San Diego Bay were performed to determine the net tidal transport of petroleum hydrocarbons. From the results, estimates of contaminant fluxes through the bay were made. The transport fluxes were compared to estimated inputs to the bay. Exchange between the bay and ocean was evaluated and residence times for various portions of the bay were estimated.

METHODS

In the studies described in this paper, a combination of flow and tracer measurements were used to estimate net tidal contaminant fluxes through cross sections of San Diego Bay. The cross sections were located at five stations in the bay including the mouth (M), Shelter Island (SI), Harbor Island (HI), Coronado Bridge North (CBN), and Coronado Bridge South (CBS), (Figure 1).

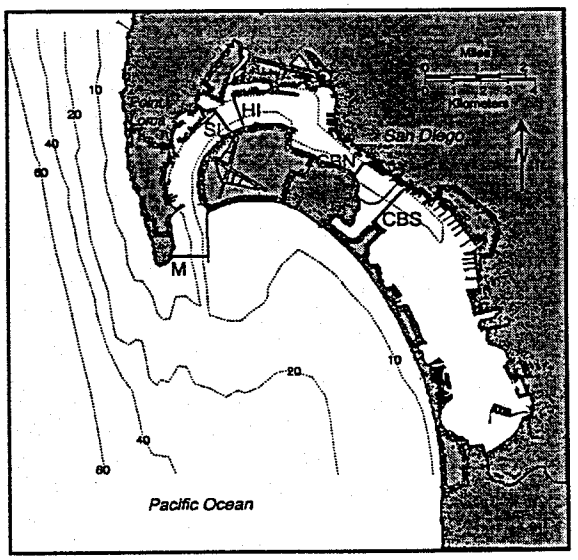

Figure 1. Map of San Diego Bay showing the location of the cross sectional transects.

The measurements at M were performed on 18 May, 1994, at SI and HI on 28 June, 1994, and at CBN and CBS on 23 August, 1994. At each section, transects were repeated at regular intervals during an approximately symmetrical semi-diurnal tide. At M, the transect interval was about every 20 minutes, while at SI, HI, CBN and CBS, the transect interval was about one hour because two stations were performed on the same tide. Figure 2 shows the predicted tidal height and time of transect for each station.

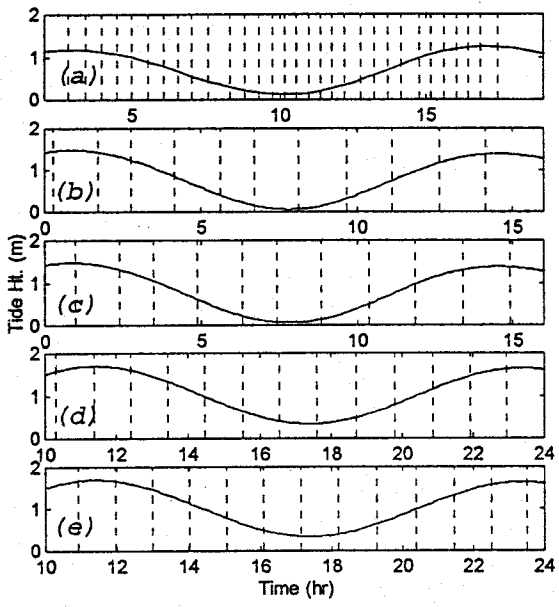

Figure 2. Tidal conditions and transect times for (a) station M, (b) station SI, (c) station HI, (d) station CBN, and (e) station CBS.

Flow Measurements: Flow measurements at each station were made using a narrow-band, 1.2 MHz ADCP mounted downward looking in a transducer well aboard the RV ECOS. The ADCP was operated in a bottom-tracking mode with a ping rate of 6 Hz and a 20 ping averaging period giving an estimated short-term velocity precision of about 3 $cm \cdot s^{-1}$. (RD Instruments, 1988). The overall sampling rate including water column averaging and bottom tracking was about 0.1 Hz. Based on the vessel speed of about 2 knots (1 $m \cdot s^{-1}$), the horizontal resolution of the flow measurements was about 10 m. The vertical resolution of the ADCP was one meter. An ~1.5 m range near the surface, and an ~1-2 m range above the bottom could not be resolved by the ADCP. Figure 3 shows the coverage from a typical ADCP cross section at station M. The ADCP data were interpolated spatially across the section using a standard 2-D Kreiging routine (Keckler, 1994). Sectional-mean residual velocity differences from the interpolation were in the range of ~0.05 $cm \cdot s^{-1}$. Bottom-boundary velocities were forced to zero by adding zero values at the bottom based on the bathymetric profiles (Innerspace 445) prior to interpolation. Lateral positions during the surveys were determined using a differential-mode Global Positioning System (DGPS) system with precision of about 2-5 m (Trimble 4000-RL2). Velocities were extended to the surface with no boundary constraint.

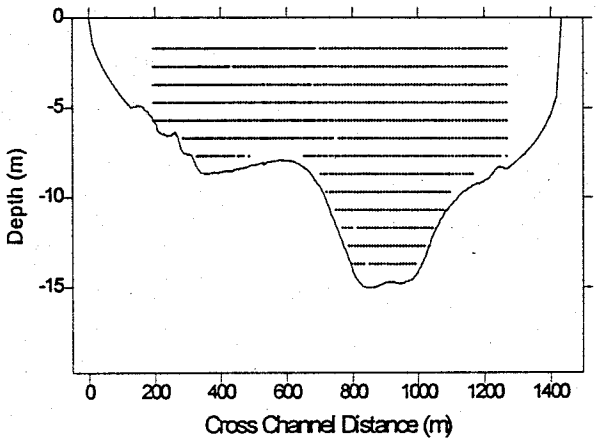

Figure3. Typical cross sectional ADCP sampling coverage at Station M.

Tracer Measurements: Hydrographic and contaminant data were obtained from a suite of towed sensors including temperature, salinity, measurement depth, transmission, pH, dissolved oxygen, and flow-through sensors including UVF and chlorophyll-a. The hydrographic data was used primarily to evaluate the local density structure and its influence on the flow, while the tracer measurements, especially the UVF were used to evaluate contaminant transport through the section. The CTD system was a standard Seabird Seacat SBE-19 fitted with a Sea-Tech 25 cm. transmisometer, and a combined DO/pH sensor. The CTD was connected to the boat by a telemetry cable which included a 25 mm ID teflon hose through which water was pumped with a magnetically-coupled centrifugal deck pump to the flow-through sensors. The towed sensors and water intake were profiled along a preset tow-yo course by paying-out and hauling-in on the tow cable with a hydraulic winch. A V-fin depressor maintained tension on the tow-body during profiling operations. The winch operator observed the vertical

and lateral position on a screen and adjusted the depth as required to maintain the desired course. A typical tow-yo cross section from the mouth is shown in Figure 4. Data from the towed sensors was logged directly to the acquisition and processing system along with DGPS data.

Water pumped from the towed array was passed through a bubble trap and into the UVF and Chl-a fluorometers. Fluorometer data were recorded onto the data acquisition system and a delay correction was made to account for time lag in the hose. The UVF measurements have been shown to provide a sensitive bulk estimate of total polycyclic aromatic hydrocarbons (TPAH) in water (Katz et al., 1991). The UVF fluorometer used in these studies was identical to that used in Katz et al. (1991) and is described in detail in that paper. Hydrographic and tracer data were processed in a similar manner to the flow data except that values were not forced to zero at the bottom boundary. Based on a profiling rate of ~5 m·min^{-1} and a sampling rate of 0.5 Hz, the vertical resolution of the data was about 6 samples·m^{-1}. The horizontal resolution was generally determined by the number of profiles performed during the cross section. This ranged from 12 at station M to 8 at station CBN. The average spacing between profiles for all the stations was about 100 m.

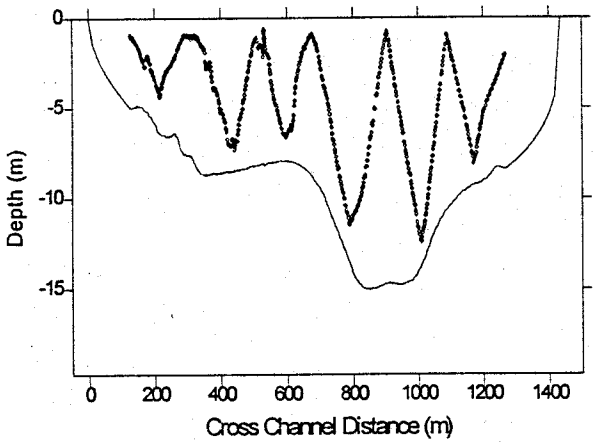

Figure4. Typical cross sectional tow-yo profile at Station M at the mouth of San Diego Bay. Depths are from the CTD and lateral positions are from the DGPS.

RESULTS & DISCUSSION

Results from typical cross sections for flow, temperature and UVF at station M are shown in Figure 5. The flow sections show several interesting points. During the ebb tide, the flow begins along the eastern channel and then fills westward toward the Point Loma shore. The ebb flow displays a strong vertical shear, and during the transition form ebb to flood, a period of two-way vertical exchange is seen. The flood tide flow is much more uniform in the vertical. The temperature sections show that the near the mouth, stratified conditions prevail and it seems clear from the vertical shear and exchange in the flow that the stratification exerts some influence over the flow (see Chadwick et al., 1995). The UVF sections at station M show that concentrations are highest in the surface layer during the ebb. Levels increase during the ebb flow as high concentration bay water is transport out of the bay. On the reversal to flood, levels initially drop along the shores as high concentration water continues to move out through the mid channel region. As the flood tide develops, overall levels drop substantially and maximum levels are observed in a mid depth region of the sections.

To evaluate contaminant transport at each station, the product of the flow and UVF concentration was integrated over the tidal cycle. Using the sectionally-interpolated flow and UVF data, the transport was integrated numerically according to

$$T_{uvf}(t) = \int_0^t \int_0^b \int_0^{h(y,t)} U(y,z,\tau) C_{uvf}(y,z,\tau)\, dz\, dy\, d\tau$$

where $T_{uvf}(t)$ is the transport of UVF through the section from time zero (slack flood) to time t, U is the water velocity, C_{ufv} is the UVF concentration, h is the water depth, and b is the channel width. Results of this integration are shown in Figure 6 where the time axis has been normalized to the semi-diurnal tidal period.

Two aspects of the transport are apparent from the results in Figure 6. First, the net transport at the end of the tidal cycle is approximately the same at each section ranging from a low of 161 kg·tide^{-1} at station CBN to 238 kg·tide^{-1} at station CBS with an average value for the 5 stations of 202 kg·tide^{-1} and a relative standard deviation (RSD) of about 16% between stations (Table 1). This suggests that inputs to the bay are fairly constant in time, and that the transport of the dissolved hydrocarbons measured by UVF is roughly conservative.

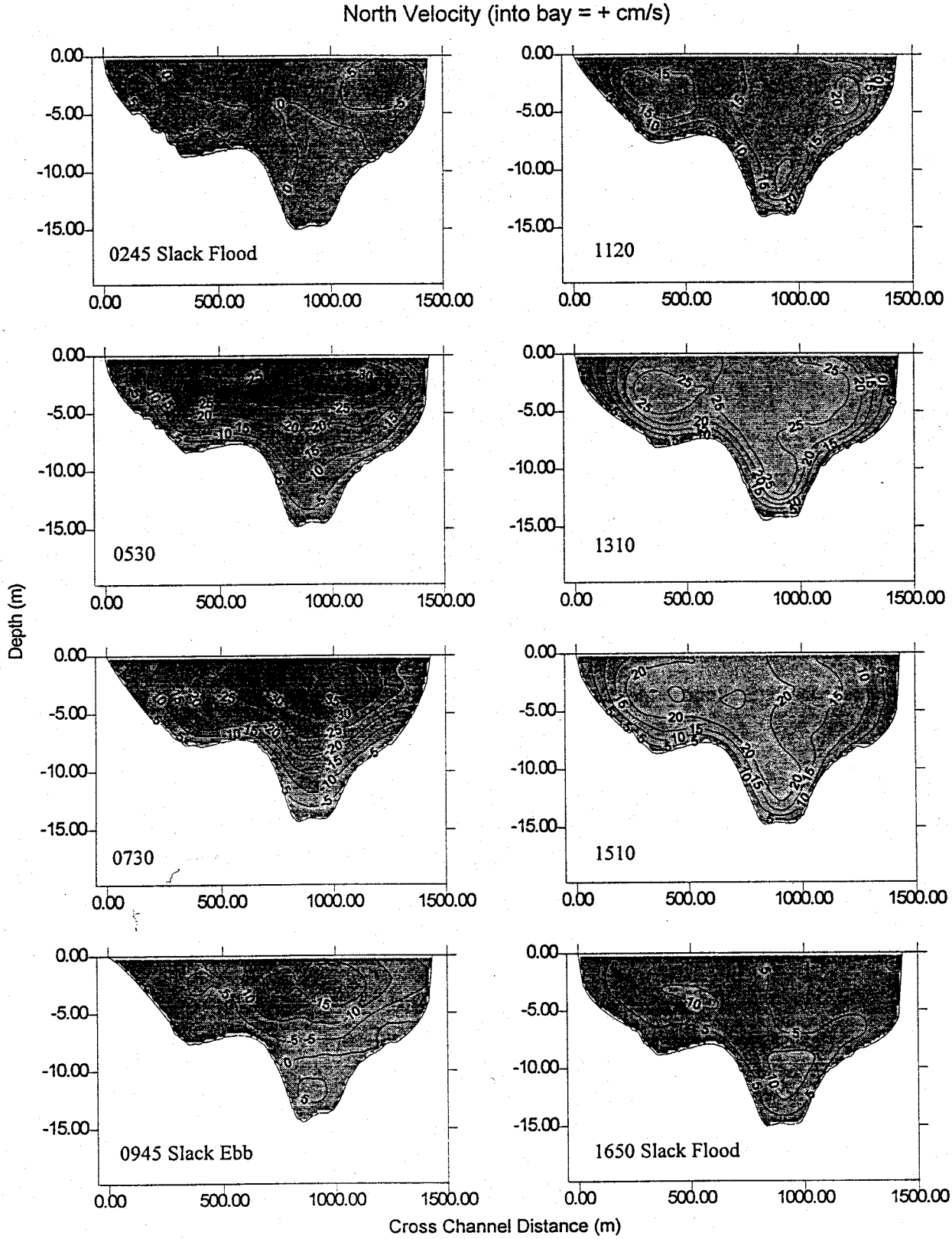

Figure 5(a). Cross sectional contours of along channel flow at Station M near the mouth of San Diego Bay.

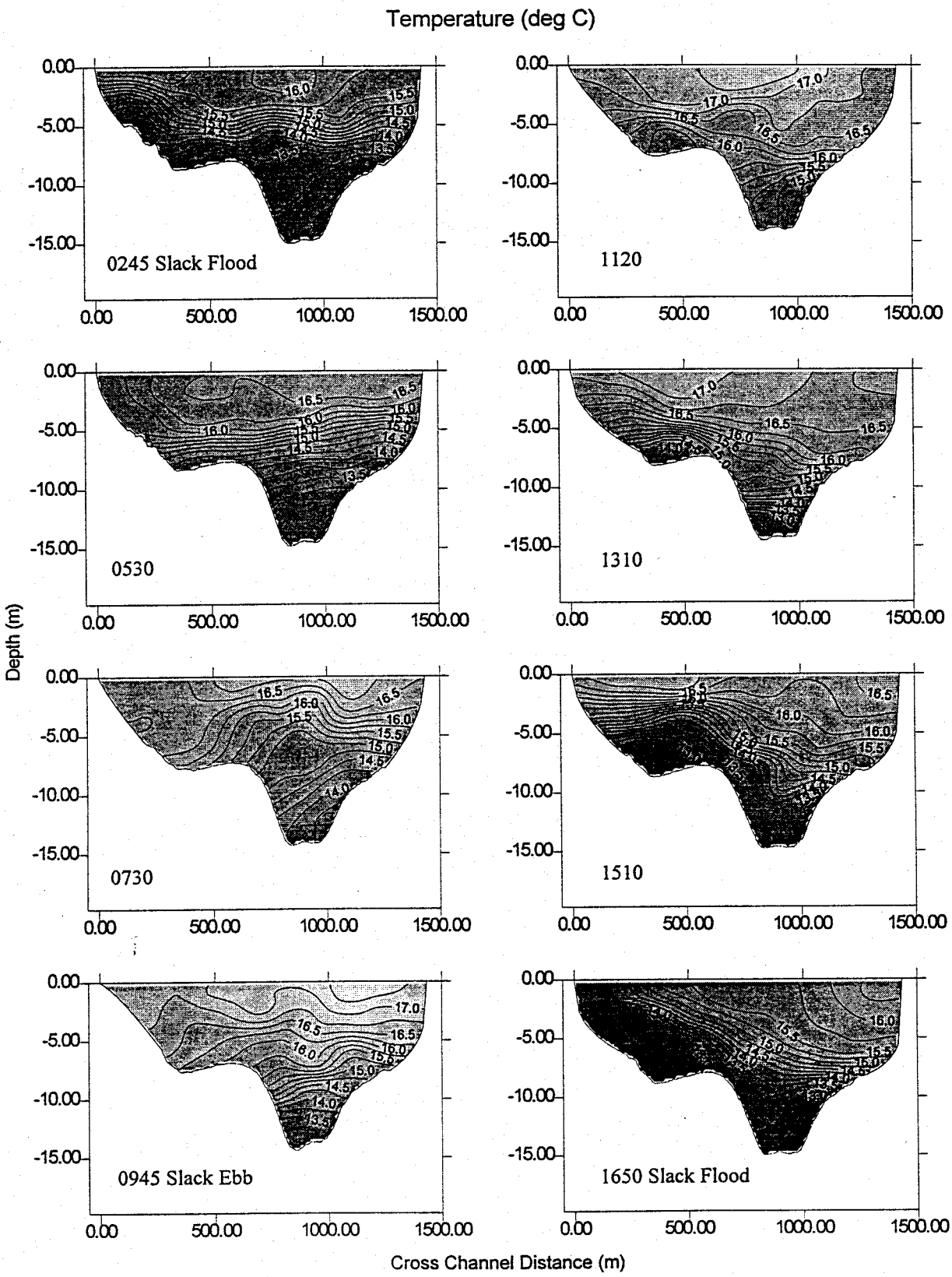

Figure 5(b). Cross sectional contours of temperature at Station M near the mouth of San Diego Bay.

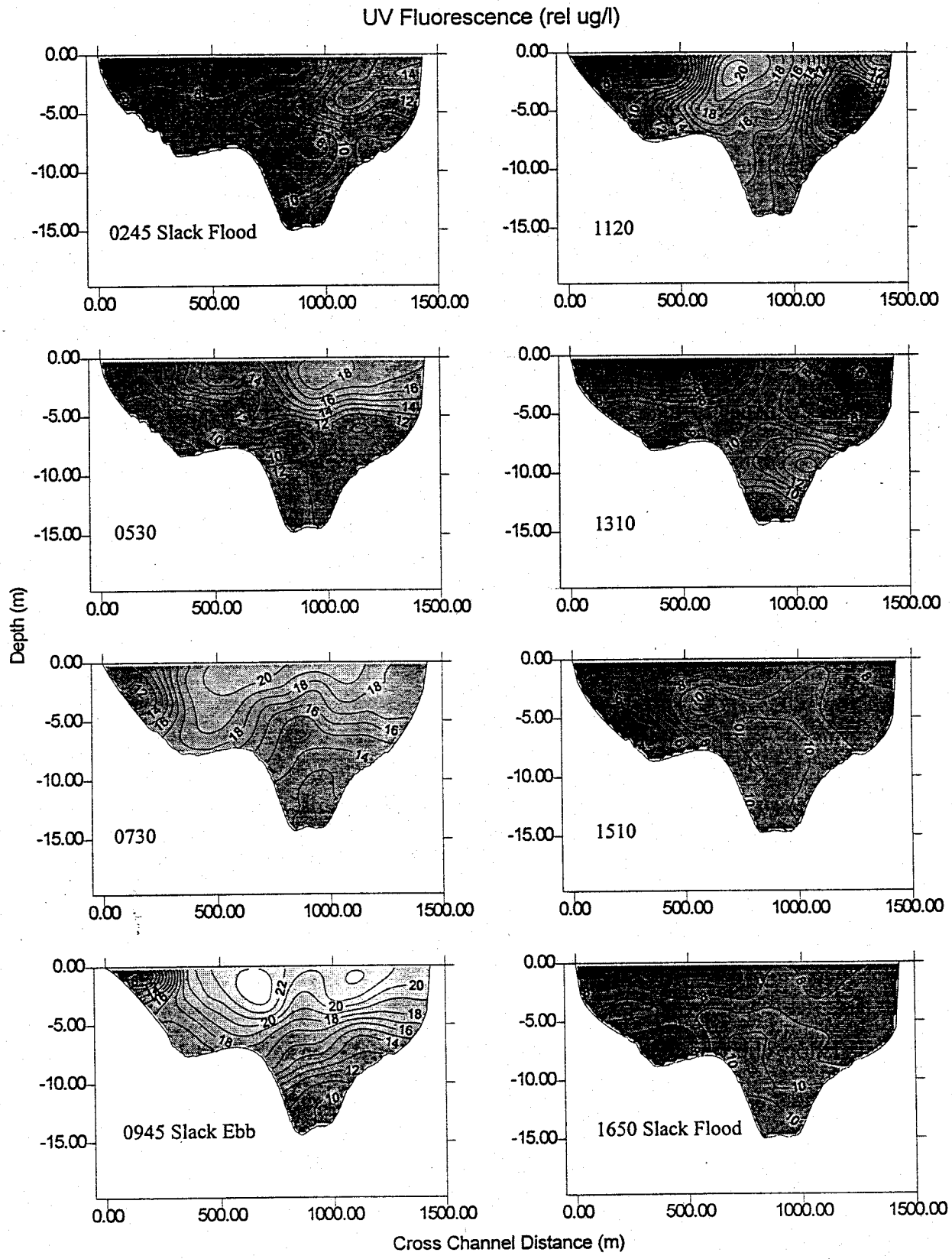

Figure 5(c). Cross sectional contours of UVF at Station M near the mouth of San Diego Bay.

Station	UVF Transport (kg/tide)	TPAH Transport (kg/tide)	TPAH Export (mt/year)	% of Input Sources
M	223	1.8	1.3	54
SI	214	1.8	1.3	54
HI	174	1.4	1.1	44
CBN	161	1.3	1.0	41
CBS	238	2.0	1.4	60
Average	202	1.7	1.2	51
%RSD	16	16	16	16

Table 1. *Net tidal transport of UVF and TPAH, annual TPAH export from the bay to the ocean, and percent of annual inputs to the bay at the five stations in San Diego Bay.*

The net tidal transport of TPAHs can be estimated based on the relationship between UFV and TPAH concentration from Katz et al. (1991)

$$C_{TPAH}\,(ng \cdot L^{-1}) \approx 8.3 \cdot C_{uvf}\,(\mu g - dfme \cdot L^{-1})$$

where C_{TPAH} is the concentration of the sum of 16 priority pollutant PAHs and their alkylated homologues, and C_{uvf} is measured against a marine diesel fuel (dfm) standard in units of dfm equivalents (dfme). Using this relation, we estimate an outward (bay to ocean) transport of TPAH ranging from 161 kg·tide^{-1} at station CBN to 238 kg·tide^{-1} at station CBS with an average value for the five stations of 1.7 kg·tide^{-1} (Table 1).

Since the measurements were performed during periods of average tidal range, the results can be extended to annual budget estimates by multiplying by the number of semi-diurnal tides in a year. This gives an average annual outward transport of TPAH from San Diego Bay of about 1.2 mt·year^{-1}. This transport represents about 50% of the estimated 2.4 mt·year^{-1} annual input to south San Diego Bay (where sources are concentrated) from all sources including fuel spills, ship discharges, stormwater, creosote pilings and aerial deposition based on source measurements and modeling (NRaD unpublished data).

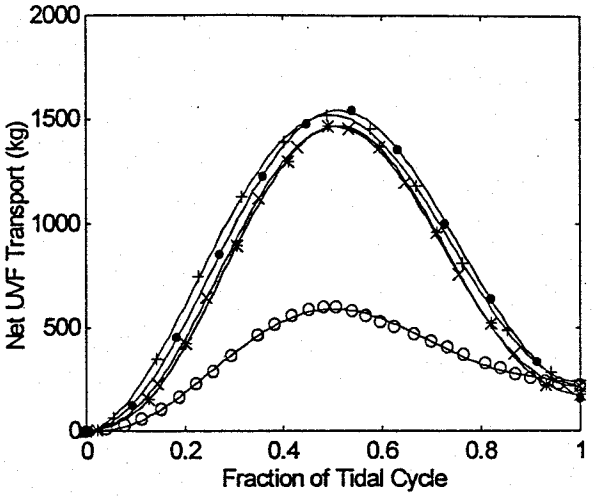

Figure 6. *Integrated tidal transport of UVF at the three stations in San Diego Bay. The time scale is normalized to the semi-diurnal tidal period for each survey. Symbols are (o) for station M, (x) for station SI, (*) for station HI, (+) for station CBN, and (•) for station CBS.*

The second characteristic of the transport that can be evaluated from the results is the tidal exchange ratio (TER) at each of the stations (Fischer et al., 1979). The TER is defined as the ratio of ocean water to total water entering the bay during the flood tide. This can be written in the form

$$TER = \frac{C_f - C_e}{C_o - C_e}$$

where C_f is the average concentration of the water entering the bay on the flood tide, C_e is the average concentration of the water leaving the bay on the ebb tide, and C_o is the concentration of the ocean water. The TER can be evaluated graphically from Figure 6 as the ratio of the net tidal transport to the peak tidal transport. Using this analysis, the TER was found to range from a high of 41% at station M, to a low of 4.2% at station CBN (Figure 7). Thus at station M near the mouth, approximately 41% of the water brought in by the flood tide is new, uncontaminated ocean water, while at station CBN only 4.2% is new water. It is clear from this analysis that the exchange drops off rapidly as a function of distance from the mouth.

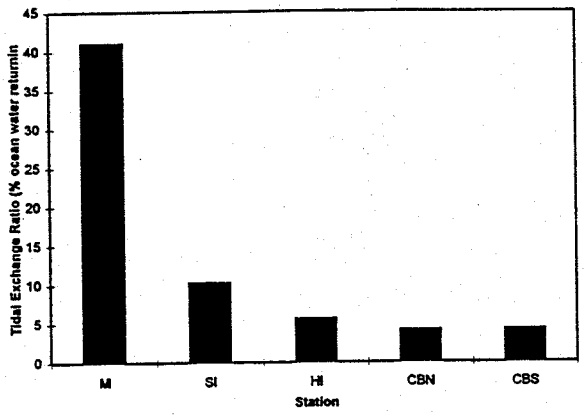

Figure 7. Measured tidal exchange ratios (TER) at the five stations in San Diego Bay. Note the large reduction in tidal exchange between the mouth station (M) and the Shelter Island station (SI) which lies at ~1 tidal excursion inside the bay.

The TER can be used to provide an estimate of the residence time for the portion of the bay inward from the measurement section. Assuming the measured TERs are representative of average tidal exchange, the residence time can be estimated from

$$\frac{C}{C_o} = \left(1 - \frac{\Delta_{tide} TER}{\Delta_{bay}}\right)^{-\left(1-\frac{\tau res}{T_{tide}}\right)}$$

where C is the time dependent concentration, C_o is the starting concentration, Δ_{tide} is the tidal prism, Δ_{bay} is the bay volume, T_{tide} is the tidal period, and τ_{res} is the residence time. Estimated residence times based on this relation and a concentration reduction of C/C_o=1/e are plotted in Figure 7.

The results show that the residence time for the entire bay (inward from station M) is about 5 days, while the residence time for the inner bay (inward of station CBN) can be as much as 38 days. The residence time increases rapidly between the mouth of the bay and the next station in at Shelter Island. This outer region of the bay is within one tidal excursion of the mouth and thus tends to be flushed on every tide. Moving into the bay beyond the first tidal excursion (~5 km for San Diego Bay), the decrease in exchange and consequent increase in residence time indicate that movement of ocean water into the deeper parts of the bay is limited by mixing rates within the bay. A natural divide between bay and ocean conditions can thus be expected to exist at the inward extent of the tidal excursion near the Shelter Island station.

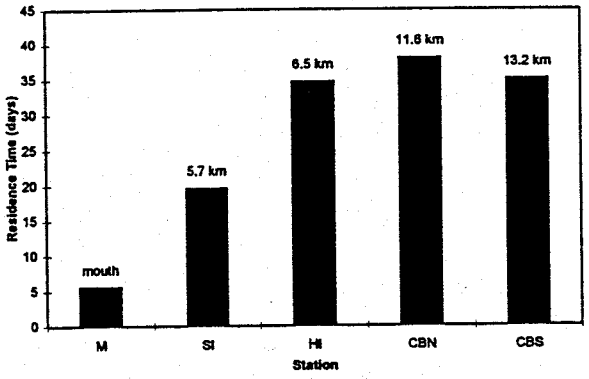

Figure 8. Estimated residence times for the regions of San Diego bay inward from the measurements stations M, SI, HI, CBN and CBS. Notes that distances are kilometers from the mouth, residence times are for the bay region beyond the distance specified, and residence times are based on a concentration reduction to 1/e of starting concentration.

CONCLUSIONS

A unique method for direct measurement of contaminant transport from a bay was demonstrated using ADCP measurements of flow and real-time UVF measurements of petroleum hydrocarbons. The results indicate that

1. Reasonable estimates of contaminant transport in bays and harbors can be obtained using a combination of flow and contaminant profiling techniques.

2. The net tidal transport of TPAH from San Diego Bay is about 1.7 kg·tide^{-1}, resulting in an estimated annual export from the bay to the ocean of about 1.2 mt·year^{-1}. This export represents about 50% of the estimated input to the bay.

3. The tidal exchange ratio for the bay ranges from a high of about 41% near the mouth to a low of about 4.2% at the Coronado bridge indicating a large variation in flushing rates for the outer bay versus the inner bay.

4. The estimated residence time for the entire bay is about 5.6 days while the residence time of the inner bay (inside CB) could be as much as 38 days.

REFERENCES

Chadwick, D.B., and Salazar, M. 1991. Integrated measurement technologies for monitoring the marine environment. Proceedings of Oceans '91, Honolulu, HI, 1:343-350.

Chadwick, D.B., Largier, J.L. and Cheng, R.T. 1995, The role of thermal stratification in tidal exchange at the mouth of San Diego Bay. 7th Biennial Conference on Physics of Estuaries and Coastal Seas, Woods Hole, Mass. (submitted).

Fischer, H.B., List, E.J., Koh, R.C.Y., Imberger, J. and Brooks, N.H. 1979. Mixing in inland and coastal waters. Academic Press, San Diego, 483pp.

Katz, C.K. and Chadwick, D.B. 1991. Real-time fluorescence measurements intercalibrated with GC-MS. Proceedings of Oceans '91, Honolulu, HI, 1:351-358.

Keckler, D. 1994. Surfer for Windows contouring and 3D surface mapping user's guide. Golden Software, Inc.

RD Instruments, 1988. Acoustic Doppler current profiler with IBM compatible data acquisition system operation and maintenance manual. p4-70.

Signell, R.P. and Butman, B. 1992. Modeling tidal exchange and dispersion in Boston Harbor. J. Geophys. Res., 97(C10):15591-15606.

Sutton, D.W., Chadwick, D.B. and Richter, K. 1995. Computer model simulations of fuel spills at Ballast Point, San Diego Bay. Proceedings of Oceans '95, San Diego, CA (this issue).

ACKNOWLEDGMENTS

This work was supported by grants from the Naval Command, Control, and Ocean Surveillance Center (#ZW865R5A01), the California Department of Boating and Waterways (IAA #93-100-026-13), and the California Regional Water Quality Control Board (IAA #1-188-190-0). Thanks to Brad Davidson, Andy Patterson, Kimball Millikan, Ron George and Gerhart Koon for assistance in field surveys and data processing.